

Enhancement of visible light emission from Tb-doped ZnO nanorods grown on silicon substrate

Kyoung-Kook Kim^a and Il-Kyu Park^{b,*}

¹Department of Nano-Optical Engineering, Korea Polytechnic University, Siheung 429-793, Korea

²Department of Materials Science and Engineering, Seoul National University of Science and Technology, Seoul 139-743, South Korea

We report on the enhancement of visible light emission from Tb-doped ZnO nanorods (NRs) fabricated on Si substrates using a simple hydrothermal process without post-thermal annealing. Structural and chemical investigations revealed that the Tb atoms were successfully incorporated into the ZnO crystal lattice without forming Tb-related alloys or impurities. Photoluminescence spectra show the typical double spectral shape of ZnO nanostructures with emission bands in the UV and visible spectral range. The visible light-emission increased linearly with the Tb-content in the solution. The emission mechanism was verified based on the energy band structure of the Tb-doped ZnO NRs.

Key words: Nanomaterials, Luminescence, Zinc oxide, Optical materials, Hydrothermal synthesis.

Introduction

Semiconductor nanostructures have attracted much attention because of the novel physical phenomena and the expected performance enhancement when shrinking dimensions of materials. ZnO-based II-VI semiconductor nanostructures have been regarded as one of the most fascinating material system mostly due to the easy control of its various shapes and large variety of applications. Therefore, ZnO-based nanostructures have been regarded as basic building block for wide variety of applications, such as optoelectronic, electronic, chemical, and energy conversion devices [1-4]. ZnO in particular has excellent physical properties, including large exciton binding energy (60 meV) and strong piezoelectric and pyroelectric coefficients originating from the large electromechanical coupling [1-4]. In addition, it can easily form the one-dimensional structures, including nanorod, nanowire, and nanoribbon structures because of its wurtzite crystal structure [1]. Three-dimensional or two-dimensional nanostructures can also be formed simply by controlling the surfactant during growth. In particular, ZnO with a large band gap of 3.3 eV has the potential of a suitable host material for the doping of rare-earth and transition metal ions. Therefore, by coupling with various rare earth elements, such as Ce, Y, Tb, Sm, and Eu, the potential applications can be expanded to novel biological and optoelectronic devices [5-10]. Among them, Tb has been used as a

dopant for green-emitting inorganic materials [9,10]. Tb-doped ZnO materials have been reported by a few groups based on wet synthesis methods, which has advantages of simplicity, easy-control, and low-temperature process [9,10]. However, the reported Tb-doped ZnO nanostructures are in the form of free-standing powders and require a thermal annealing after synthesis to achieve efficient luminescence [9, 10]. To simplify the process and to expand the range of applications, ZnO nanostructures could be controlled on a rigid substrate without requiring a post-thermal annealing process. In this paper, we report on Tb-doped ZnO nanorods (NRs) grown on a silicon substrate using a low-temperature hydrothermal method without thermal annealing. The Tb-doped ZnO NRs show enhanced emission at visible wavelength.

Experimental

A *p*-type Si (100) wafer was used as a substrate to grow Tb-doped ZnO NRs after removing all organic contaminants using a mixed solution of NH₄OH (30%)/H₂O₂ (30%)/H₂O (1 : 1 : 5, v/v) at 60 °C for 30 min. A seed layer for the ZnO NRs was formed by dipping the substrate into a 60 mM zinc acetate dihydrate (Zn(CH₃COO)₂·2H₂O) solution in ethanol at 80 °C, followed by drying at 100 °C for 5 min. This process was repeated three times to increase the chance for formation ZnO nuclei and to cover the whole surface completely with the ZnO seed layers.

The Tb-doped ZnO NRs were grown by placing the seed layer-grown substrate into a mixed solution of 30 mM zinc nitrate hexahydrate (Zn(NO₃)₂·6H₂O), 30 mM hexamethylenetetramine ((CH₂)₆N₄; HMT), and

*Corresponding author:
Tel : +82029706349
Fax: +82029736657
E-mail: pik@seoultech.ac.kr

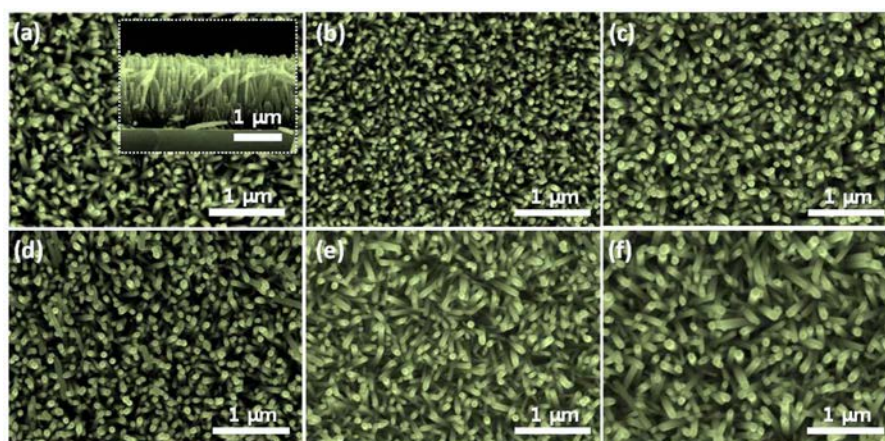


Fig. 1. FE-SEM images of (a) undoped (0%), (b) 1% Tb-doped, (c) 3% Tb-doped, (d) 10% Tb-doped, (e) 20% Tb-doped, and (f) 30% Tb-doped ZnO NRs.

various concentrations of terbium nitrate hexahydrate ($\text{Tb}(\text{NO}_3)_3 \cdot 6\text{H}_2\text{O}$) in DI water at 90 °C for 3 hrs. The amount of the Tb source was varied from 0 to 30% of the molarity of the Zn source. At solution temperatures above 70 °C, the solution became cloudy, indicating that the chemical reaction had started. The color of the solution changed from white to yellow and then to orange with increasing Tb content from 0 to 30%. After the reaction, the samples were cleaned with DI water in an ultrasonic bath for 5 min to completely remove the free-standing ZnO nanostructures.

The morphological properties of the Tb-doped ZnO NRs were characterized by field emission scanning electron microscopy (FE-SEM). The chemical composition of the Tb-doped ZnO NRs was measured by energy dispersive X-ray (EDX) spectroscopy attached to the FE-SEM. High-resolution X-ray diffraction (HR-XRD) was used to obtain the information about crystallographic structures. The optical properties were investigated by photoluminescence (PL) spectra, which were measured using a 24-mW power 325-nm continuous He-Cd laser at room temperature. The laser was focused onto the sample surface using an objective lens. The excitation area was approximately 400 μm in diameter.

Results and Discussion

Fig. 1 shows the surface morphology of the undoped and Tb-doped ZnO NRs obtained with the various Tb concentrations. The diameter and length of the undoped ZnO NR were around 50 nm and 1.6 μm , respectively, as shown in Fig. 1(a). With Tb concentration over 20%, the diameter increased slightly compared to the undoped ZnO NRs, as shown in Figs. 1(e) and 1(f). All the ZnO NRs were closely packed and vertically aligned with a similar shape of well-faceted six-sided surfaces and a hexagonal top facet. Therefore, the morphology of the ZnO NRs did not change significantly with the amount of Tb-doping agent. This indicates that the growth is not influenced by the Tb doping because the content of the

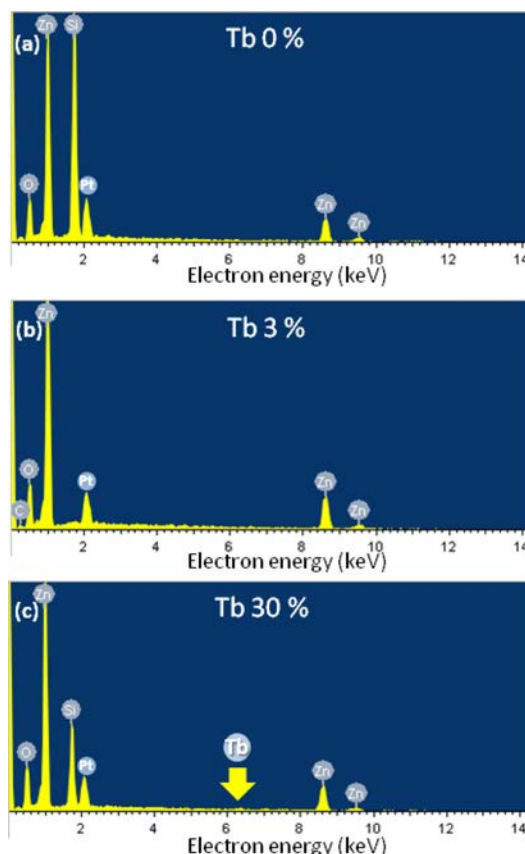


Fig. 2. EDX spectra of (a) undoped (0%), (b) 3% Tb-doped, and (c) 30% Tb-doped ZnO NRs.

dopant agent was too small compared to the ZnO source to change the morphology.

Figs. 2(a-c) show the EDX spectra of the undoped, 3%, and 30% Tb-doped ZnO NRs. All spectra show peaks corresponding only to Zn and O in the ZnO NRs, as well as Si and Pt peaks corresponding to the substrate and coating material for SEM measurement. No additional peak was observed in the EDS patterns of the undoped and Tb-doped ZnO NRs. This indicates

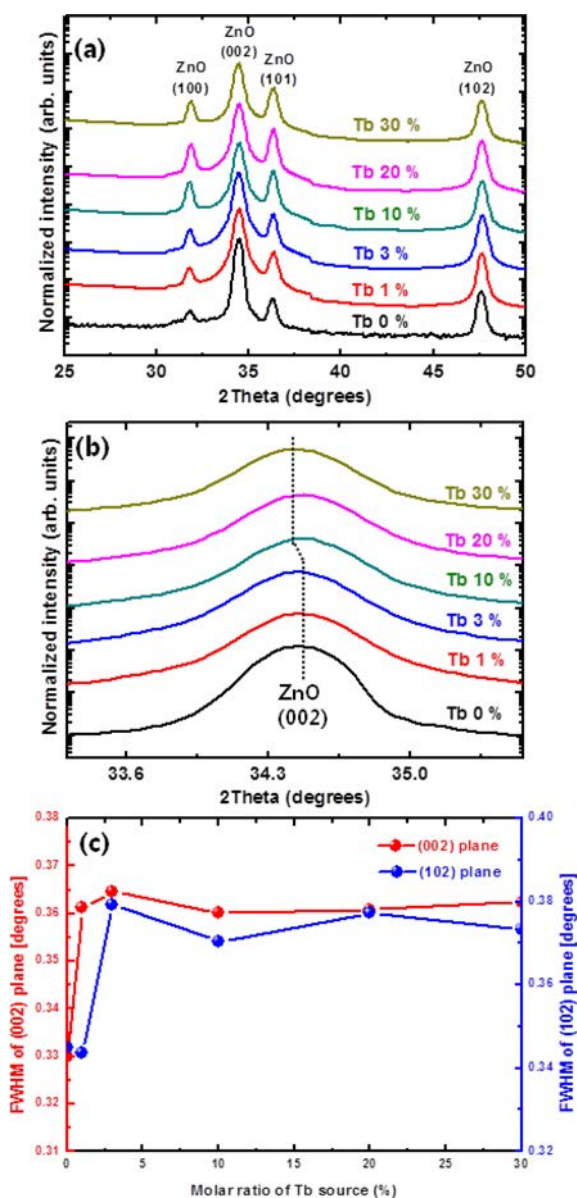
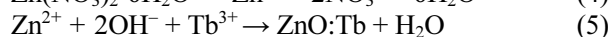
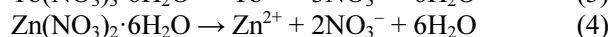
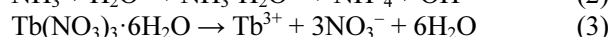
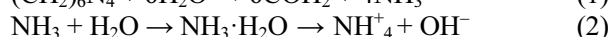


Fig. 3. (a) Normalized θ - 2θ XRD patterns of undoped and Tb-doped ZnO NRs with different Tb source concentrations in the solution. (b) Variation of ZnO (002) peak position with variation of the Tb-doping concentration. (c) FWHM of (002) and (102) diffraction peaks with variation of Tb molar contents in the solution.

that Tb-related alloys or precipitates are not formed during the growth of the Tb-doped ZnO NRs. At 30% concentration, there is a small peak corresponding to Tb, indicating that Tb was successfully incorporated into the ZnO NRs.

To investigate the crystal structure of ZnO NRs, HR-XRD was measured for the Tb-doped ZnO NRs. Fig. 3(a) shows full-range XRD patterns of the undoped and Tb-doped ZnO NRs with various source concentrations. The diffraction patterns are in agreement with the bulk wurtzite structure of ZnO (space group: P6₃mc; $a = 0.0.32501$ nm, $c = 0.52071$ nm, JCPDS 79-2205). The diffraction peaks correspond to the (100), (002), (101),

and (102) planes of hexagonal ZnO crystal. There were no diffraction peaks except those for ZnO. This indicates that no other chemical species formed, including Tb oxide or Zn-Tb alloys. Fig. 3(b) shows the variation of (002) peaks. As the Tb-content increases, the (002) peaks shifted toward lower angle compared to the undoped ZnO NR. This is related to the change of the inter-atomic distance, which can be explained by Bragg's law for X-ray diffraction, $2d \cdot \sin\theta = n\lambda$, where d is the inter-plane distance, θ is the diffraction angle, n is an integer number, and λ is the wavelength of the X-ray source. Based on Bragg's law, the shift of the diffraction peak to a lower angle means an increase of the inter-atomic distance of the (002) plane. This can be attributed to the slightly increased lattice size of the ZnO as a result of Tb doping because of the larger ionic radius of Tb³⁺ (1.18 Å) than Zn²⁺ (0.74 Å). Because of this large difference in radius, the incorporation of the foreign element would be hindered, even though the source concentration was very large around 30%. Fig. 3(c) summarizes the full-width at half maximum (FWHM) of the (002) and (102) planes with variation of the Tb content. It is well known that the FWHM of the (002) and (102) diffraction peaks in hexagonal crystal structure implies the quantity of crystal defects or distortion in the lattice structure. Compared with the undoped ZnO NRs, the Tb-doped ZnO NRs showed increased FWHM for both peaks. However, among the Tb-doped NRs, there was no significant difference between them for different Tb content. This indicates that the crystal defects or distortion in lattice structure were increased by the Tb doping, but the crystal quality was not affected by the Tb content. Even though the Tb content in the solution is large over 30%, the incorporation of Tb into the ZnO lattice would be limited due to the large difference in size between substitutional Tb³⁺ and the host Zn²⁺ ions. The mechanism for the formation of Tb-doped ZnO NRs can be summarized by the following reaction:



In the reaction, the HMT supplies OH⁻ ions to the cations to form metal oxides [11]. Thus, the Tb³⁺ ions can substitutionally incorporate into the Zn sites during the ZnO NR growth.

To investigate the optical properties, we measured the PL spectrum at room temperature using a 325-nm He-Cd laser as an excitation source. Fig. 4(a) shows the PL spectra of the undoped and Tb-doped ZnO NRs for the full spectral range. The PL spectra for all samples show two emission peaks: a sharp peak at 380 nm in the UV range and broad one covering the whole

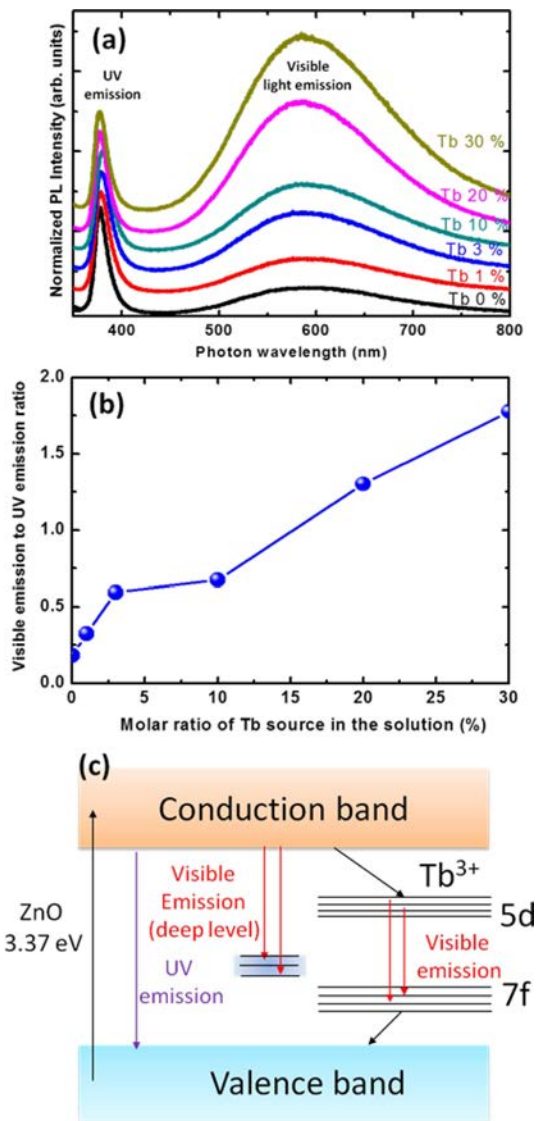


Fig. 4. (a) Normalized PL spectra of the as-grown ZnO NRs measured over full spectral range. (b) Intensity ratio of visible light emission to UV emission with variation of Tb molar content in the solution. (c) Schematic energy level diagram of the Tb^{3+} electronic levels in the ZnO bandgap.

visible spectral range from 450 to 800 nm. This spectral shape is typical for ZnO nanostructures synthesized by wet chemistry methods [12, 13]. The sharp peak in the UV region is assigned to the band edge emission of the ZnO crystal, and the broad emission peak in the visible range is attributed to radiative recombination through point defects in the ZnO lattice, such as oxygen vacancies, zinc vacancies, oxygen interstitials, zinc interstitials, and anti-site defects [12, 13]. In the case of Tb-doped ZnO NRs, however, the visible emission is enhanced with increasing Tb content. Fig. 4(b) shows that the intensity ratio of the visible light emission to the UV emission increases with the Tb source in the solution. This indicates that the visible light emission is enhanced with increasing Tb-doping concentration. As shown in Fig. 4(c), there

are two emission processes for the visible light emission of the Tb-doped ZnO NRs: one is a well-known ensemble of deep levels originating from various point defects, and the other is the atomic transitions of the Tb^{3+} dopants in the ZnO lattice. It is difficult to obtain information from the Tb^{3+} spectra on the nature of the Tb^{3+} center due to the high degeneracy of the Tb^{3+} levels involved in several transitions [9, 10]. However, considering the selection rules, the possible transitions are mainly 5d_3 and $^5d_4 \rightarrow ^7f_J$ ($J=6, \dots, 0$) transitions of Tb^{3+} , which are called the low-energy ground state and excited states, respectively [9, 10]. These transitions correspond to the emission lines at around 490 to 620 nm, which is very close to the emission bands by defect-related deep-level emission of the ZnO crystal. In the spectra, the emission peak showed a very broad band. This is due to the overlapping of emission bands from both several defect-related deep-level emissions and the atomic transitions from the Tb^{3+} dopants [14]. As shown in the HR-XRD results in Fig. 3(c), the amount of defects in the ZnO lattice did not increase with increasing Tb content in the solution from 3 to 30%. Therefore, the enhancement of visible light emission is attributed to the atomic transitions from the Tb^{3+} dopants. It should be noted that the visible light emission was enhanced just by doping the Tb into the ZnO NRs without post-thermal annealing processes. This implies that the Tb-doped ZnO NRs can be applicable to active media in optoelectronic devices, such as light-emitting or converting devices.

Conclusions

We have reported on the fabrication of Tb-doped ZnO NRs and the enhancement of visible light emission by the doping without a post-thermal annealing process. The Tb-doped ZnO NRs were grown on controllable Si substrates using a simple hydrothermal process. Structural and chemical investigations by using FE-SEM, HR-XRD, and EDX results showed that the Tb was successfully incorporated into the ZnO crystal lattice and unwanted Tb-related impurities or alloys did not form. The room temperature PL spectra showed a typical shape of ZnO nanostructures with a sharp emission peak in the UV range and a broad emission band at visible spectral range. However, the visible light-emission was linearly increased with increasing the Tb-contents in the solution. The emission mechanism was verified based on the energy band structure of the Tb-doped ZnO NRs. These results suggest that the Tb-doped ZnO nanostructures fabricated by this simple approach allow for control of the emission wavelength, which makes them applicable in light-emitting devices.

Acknowledgments

The authors especially thank to Mr. Md Roqibul

Hasan (Yeungnam University) for assistance with the experiments. This study was supported by the Basic Science Research Program (NRF-2014R1A2A1A110 54154) through the National Research Foundation of Korea funded by the Ministry of Science, ICT and Future Planning of the Korean government.

References

1. S. Xu and Z.L. Wang, *Nano Res.* 4 (2011) 1013-1098.
2. Z.L. Wang and J. Song, *Science* 312 (2006) 242.
3. J.H. Koo and B.W. Lee, *J. Ceram. Process. Res.* 18 (2017) 156-160.
4. A. Umar and Y B. Hahn, *Metal oxide nanostructures and their applications: ZnO nanostructures and Nanodevices* (Los Angeles, American Scientific Publishers), 2010.
5. V.Z. Mordkovich, H. Hayashi, M. Haemori, T. Fukumura, and M. Kawasaki, *Adv. Funct. Mater.* 13 (2003) 519-524.
6. B. Cheng, Y. Xiao, G. Wu, and L. Zhang, *Adv. Funct. Mater.* 14 (2004) 913-919.
7. Y.I. Jung, S.H. Baek, and I.K. Park, *Thin Solid Films* 546 (2012) 259-262.
8. Y.I. Jung, B.Y. Noh, Y.S. Lee, S.H. Baek, J.H. Kim, and I.K. Park, *Nanoscale Res. Lett.* 7 (2012) 43.
9. Y.H. Yang, H.G. Zhu, H.M. Dong, and G.W. Yang, *Mater. Lett.* 124 (2014) 32-35.
10. A. Urbieto, R. del Campo, R. Pérez, P. Fernández, and J. Piqueras, *J. All. Com.*, 610 (2014) 416-421.
11. S. Singh, I.K. Park, and S.H. Park, *J. Ceram. Process. Res.* 17 (2016) 218-222.
12. C.H. Ahn, Y.Y. Kim, D.C. Kim, S.K. Mohanta, and H.K. Cho, *J. Appl. Phys.* 105 (2009) 013502.
13. C. Wu, X. Qiao, L. Luo, and H. Li, *Mater. Res. Bull.* 43 (2008) 1883-1891.
14. Z. Kotan, M. Ayvacikli, Y. Karabulut, J. Garcia-Guinea, L. Tormo, A. Canimoglu, T. Karali, and N. Can, *J. All. Com.* 581 (2013) 101-108.